ELSEVIER

European Journal of Mechanics B/Fluids 21 (2002) 307–316

EUROPEAN JOURNAL OF MECHANICS B/FLUIDS

Three-dimensional instability of two counter-rotating vortices in a rectangular cavity driven by parallel wall motion

S. Albensoeder *, H.C. Kuhlmann

ZARM – University of Bremen, Am Fallturm, D-28359 Bremen, Germany

Received 12 June 2001; received in revised form 7 February 2002; accepted 13 February 2002

Abstract

The linear stability of two counter-rotating vortices driven by the parallel motion of two facing walls in a rectangular cavity is investigated by a finite volume method. Critical Reynolds and wave numbers are calculated for aspect ratios ranging from 0.1 to 5. This range is sufficient to find the asymptotic behavior of the critical parameters when the aspect ratio tends to zero and infinity, respectively. The critical curve is smooth for all aspect ratios and, hence, the character of the instability changes continuously. When the moving walls are far apart the mechanism is centrifugal, as in the classical lid-driven cavity. For aspect ratios near unity a combined mechanism, also involving strain near the vortex cores, leads to the instability which tends to asymmetrically displace the vortex cores, very similar to the cooperative short-wave instability of a free counter-rotating vortex pair. In the limit when plane Poiseuille flow is approached in the bulk, the three-dimensional perturbations are strongly localized near both downstream ends of the moving walls.

PACS: 47.15.Fe; 47.15.Rq; 47.20.-k

MSC: 76D17; 76E09

Keywords: Lid-driven cavity; Stability; Vortex flow

1. Introduction

The fluid motion in rectangular cavities bounded by rigid walls and driven by the tangential motion of parts of the boundaries is an excellent setup for studying fundamental hydrodynamic issues of incompressible closed flows. In particular, the classical problem of a single lid-driven cavity has been considered extensively both experimentally and numerically. Owing to its simplicity, this system is also frequently employed as a numerical benchmark for Navier–Stokes solvers [1]. Among the topics which have been studied using the lid-driven cavity are the fundamental flow structure [2], viscous corner eddies [3–5], transition to turbulence [6,7], end-wall effects [8–10], and mixing in Stokes flow [11]. A review on the single-lid-driven cavity has been provided by [12].

The instability of the two-dimensional steady flow in the one-sided lid-driven cavity has been investigated numerically by [13–16] using the assumption that the cavity is infinitely extended in the spanwise direction, perpendicular to the direction of motion of the moving wall. While [13] considered the instability of flow with respect to two-dimensional perturbations, Refs. [14–16] aimed at a three-dimensional linear stability analysis. Finally, the linear-stability problem for the classical lid-driven cavity was solved by [17] for the whole range of cavity aspect ratios. They showed that the basic flow can become unstable to four different three-dimensional modes depending on the cross-sectional geometry. Two of the unstable modes are stationary, while two other modes are oscillatory. Different to previous results it was shown that the most dangerous mode in the

* Correspondence and reprints.
E-mail address: salben@zarm.uni-bremen.de (S. Albensoeder).

0997-7546/02/$ – see front matter
PII: S0997-7546(02)01188-3

square cavity is stationary with a short wavelength. By energy-transfer considerations it was demonstrated that all instabilities are caused by centrifugal effects which are operative in different regions of the basic cavity shear flow.

Regarding flow instabilities, the classical one-sided lid-driven cavity problem has been extended to two-sided driving by [18]. When two facing walls move in parallel or anti-parallel directions different types of instabilities are possible. They arise due to the interaction of the co- or counter-rotating primary vortices that form adjacent to each moving wall. In particular, it was shown that the elliptic instability can arise for anti-parallel wall motion and for cavity aspect ratios for which the two main co-rotating vortices merge [18,19]. Blohm and Kuhlmann [20] experimentally extended the work of [18] using an apparatus in which the separation of the two moving walls was about twice the distance of the two stationary walls. They measured velocity profiles and wall shear stresses in three-dimensional steady and time-dependent flows for anti-parallel wall motion. Albensoeder and Kuhlmann [21] completed the analysis of [18] and calculated the linear stability boundaries for two-sided lid-driven cavities with anti-parallel wall motion for the whole range of aspect ratios. Depending on the aspect ratio they found four different main branches of steady instabilities. The situation is only complicated in a narrow range of aspect ratios where multiple two-dimensional states arise [22]. For large aspect ratios, i.e. for a large separation of the moving walls, the basic flow consist of two, essentially independent, co-rotating primary vortices. On an increase of the Reynolds number this state becomes centrifugally unstable, similar as in the classical cavity [17]. When the moving walls come closer to each other the two vortices merge and the instability changes to an elliptic type. Near unit aspect ratio a quadripolar instability was found and, when the gap between the moving walls becomes very narrow such that a plane Couette flow is established in the bulk, the flow is again subject to an elliptic instability. In this latter case the instability is strongly localized near both ends of the cavity where the flow is turning.

In the present paper we investigate the linear stability of the two-sided lid-driven cavity flow when the two facing walls move parallel to each other with the same speed. We inquire about the type of instability and the dependence of the critical Reynolds and wave number on the aspect ratio.

2. Problem formulation, solution method, and code validation

Consider an incompressible Newtonian fluid with kinematic viscosity ν and density ρ inside a rectangular container of width d and height h. The flow is driven by two facing walls at $x = \pm d/2$ which move tangentially in the positive y direction and with the same velocity V. The geometry of the rectangular container is sketched in Fig. 1 where we assume that the depth in z direction is infinite. By using the characteristic scales h, ν/h, $\rho\nu^2/h^2$, and h^2/ν for length, velocity, pressure, and time, respectively, the Navier–Stokes equations are given by

$$\nabla \cdot \boldsymbol{u} = 0, \tag{1}$$

$$\frac{\partial \boldsymbol{u}}{\partial t} + \boldsymbol{u} \cdot \nabla \boldsymbol{u} = -\nabla p + \nabla^2 \boldsymbol{u}, \tag{2}$$

with velocity $\boldsymbol{u} = (u, v, w)$ and pressure p. The no-slip boundary conditions on the top and bottom walls are

$$\boldsymbol{u}(y = \pm 1/2) = 0. \tag{3}$$

On the moving walls we require

$$\boldsymbol{u}(x = \pm \Gamma/2) = \mathrm{Re}\, \boldsymbol{e}_y, \tag{4}$$

where the Reynolds number is denoted by

$$\mathrm{Re} = \frac{hV}{\nu}, \tag{5}$$

and Γ is the aspect ratio

$$\Gamma = \frac{d}{h}. \tag{6}$$

The governing equations allow for a two-dimensional steady solution ($\partial/\partial t = \partial/\partial z = w_0 \equiv 0$) called the basic flow $(\boldsymbol{u}_0, p_0)$. Albensoeder et al. [22] have shown that the basic solutions are not unique for $\Gamma \sim 1$ and $\mathrm{Re} \gtrsim 350$. In addition to the solution which is symmetric with respect to the plane $x = 0$ non-symmetric solutions arise in this region of the parameter space. As will be shown later, the parameter range where multiple basic solutions arise is well beyond the three-dimensional linear stability boundary of the symmetric state which is unique for small Reynolds numbers.

The linear stability of the basic state $(\boldsymbol{u}_0, p_0)$ is governed by

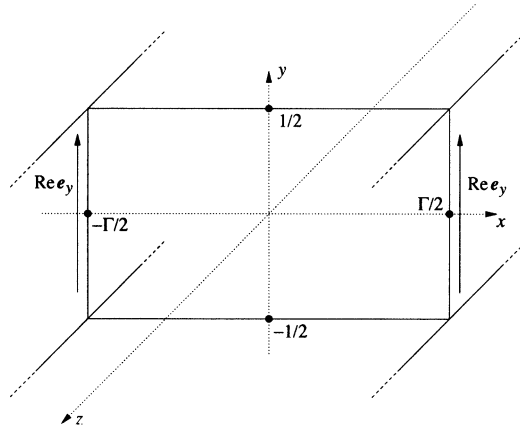

Fig. 1. Geometry of the cavity. Lengths are given in units of the cavity's height h, the velocity in units of ν/h.

$$\nabla \cdot \boldsymbol{u} = 0, \tag{7}$$

$$\frac{\partial \boldsymbol{u}}{\partial t} + \boldsymbol{u}_0 \cdot \nabla \boldsymbol{u} + \boldsymbol{u} \cdot \nabla \boldsymbol{u}_0 = -\nabla p + \nabla^2 \boldsymbol{u}, \tag{8}$$

where $(\boldsymbol{u}, p)$ denote the velocity and pressure perturbations. Since the basic flow already satisfies the boundary conditions on the walls, we are left with the homogeneous conditions for the perturbation flow

$$\boldsymbol{u}(\pm\Gamma/2) = \boldsymbol{u}(\pm 1/2) = 0. \tag{9}$$

The infinite extension of the cavity in z direction allows for solutions in the form of normal modes

$$\begin{pmatrix} \boldsymbol{u} \\ p \end{pmatrix}(x, y, z, t) = \begin{pmatrix} \boldsymbol{U} \\ P \end{pmatrix}(x, y) \exp\{\sigma t + \mathrm{i}(kz - \omega t)\} + \text{c.c.}, \tag{10}$$

where the growth rate σ, the oscillation frequency ω, and the wave number k of the perturbation are real. Inserting the ansatz (10) into (7) and (8) we get, after discretization, a generalized eigenvalue problem with eigenvalue $\sigma - \mathrm{i}\omega$ (complex growth rate) and complex eigenvector $(\boldsymbol{U}, P)$. On the neutral stability boundary the growth rate must vanish, i.e. $\sigma(\mathrm{Re}_n, \Gamma, k) = 0$. The critical mode is defined by $\max_{q,k} \sigma(\mathrm{Re}_n, \Gamma, k, q) = 0$ where $q \in \mathbb{N}$ numbers the discrete part of the spectrum.

For an analysis of the instability mechanisms we consider the Reynolds–Orr energy equation for the kinetic energy E_{kin}:

$$\frac{1}{D_*}\frac{\mathrm{d}E_{\mathrm{kin}}}{\mathrm{d}t} = -1 + \sum_{i=1}^{4} \int_V I_i \,\mathrm{d}V = -1 - \frac{1}{D_*} \int_V \left(uu\frac{\partial u_0}{\partial x} + uv\frac{\partial u_0}{\partial y} + vu\frac{\partial v_0}{\partial x} + vv\frac{\partial v_0}{\partial y} \right) \mathrm{d}V, \tag{11}$$

which has been normalized by the dissipation in the volume

$$D_* = \int_V (\nabla \times \boldsymbol{u})^2 \,\mathrm{d}V. \tag{12}$$

The local normalized energy production terms I_i are numbered consecutively as they appear in (11).

Equations (1)–(4) and (7)–(9) are discretized by a finite-volume-method, exactly as in [17,22]. The grid is slightly compressed towards the boundaries using a stretching factor between neighboring cells of 0.95. To solve the nonlinear equations for the basic state a Newton–Raphson method is employed. After convergence, the basic state is inserted into (7)–(9) to obtain an algebraic linear stability problem. The eigenvalues are calculated by inverse iteration and the resulting linear matrix problems are solved by LAPACK subroutines. The roots of the real part of the growth rate are obtained using Newton's method.

The code for the basic-flow calculations has already been validated by comparison with results for the classical one-sided lid-driven cavity [22]. Likewise, the linear-stability code has been validated in [17] by comparison with results of [15,16,18,19]. As in our previous investigations [17,21], we employ a grid resolution of 141×141 for all calculations. The difference between the critical parameters values obtained on this fine grid and those calculated on a course grid with 71×71 grid points is used as an error estimate. From this indicator the error for the critical Reynolds number is less than 4% for aspect ratios $\Gamma \leqslant 4$. At higher aspect ratios the estimated error for the critical Reynolds number is less than 6.5%. To prove grid convergence, representative critical Reynolds numbers are shown in Fig. 2 as functions of the number of grid points.

From these data, the extrapolated critical Reynolds numbers are well within our error bound. In fact, in many cases the real numerical error is considerably less than the above conservative estimate.

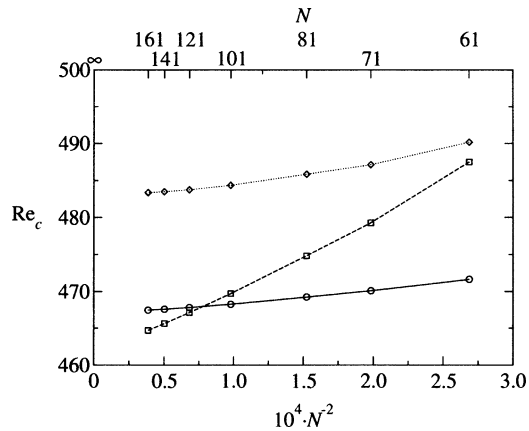

Fig. 2. Critical Reynolds numbers Re_c as a functions of the number N of grid points for each space coordinate. (◯): $\Gamma = 0.35$, (◇): $\Gamma = 1.75$, and (□): $\Gamma = 2.20$.

3. Results

3.1. Linear stability boundaries

The linear stability boundary Re_c is shown in Fig. 3 as function of the aspect ratio Γ. Throughout the full range of Γ the critical curve is smooth and contiguous and the instability is stationary. Hence, the critical mode changes continuously, as well as the instability mechanism.

For $\Gamma \to \infty$ each walls drives its own vortex. These two primary vortices with opposite sense of rotation drive secondary weak viscous eddies in the bulk whose intensity decays exponentially from both moving walls [3]. Since inertial effects are essential for any instability, the three-dimensional instability mode will be localized near the primary vortices in the vicinity of the moving walls. Because both primary vortices are nearly independent, we consistently recover, for $\Gamma \to \infty$ (Fig. 4(b)), the stability result for the flow in the classical single-lid-driven cavity [17] and in the cavity in which the two facing walls move in opposite directions [21]. For $\Gamma = 3$, e.g., the critical Reynolds number deviates only less than 9% from the estimated asymptotic value $\mathrm{Re}_c(\Gamma \to \infty) = 420 \pm 20$ ($k_c(\Gamma \to \infty) = 1.69 \pm 0.03$) [17].

For $\Gamma \to 0$ we likewise find an asymptotic behavior, shown in Fig. 4(a). Scaling all lengths by the separation of the moving walls d, which is the relevant length scale for $\Gamma \to 0$, instead of h the asymptotic critical Reynolds and wave numbers are determined with high accuracy as $\lim_{\Gamma\to 0} \mathrm{Re}_c^* = \lim_{\Gamma\to 0}(\mathrm{Re}_c\,\Gamma) = 164 \pm 6$ and $\lim_{\Gamma\to 0} k_c^* = \lim_{\Gamma\to 0}(k_c\,\Gamma) = 2.69 \pm 0.01$, respectively. For future reference, some representative numerical data are collected in Table 1.

Also given in Fig. 3 are linear stability curves for pure two-dimensional bifurcations (dotted lines) which have been computed by [22]. At this critical curve for $k = 0$ the two-dimensional steady basic flow with streamlines mirror symmetric to $x = 0$ bifurcates to a pair of steady two-dimensional flows with broken mirror symmetry. The bifurcation is supercritical along the

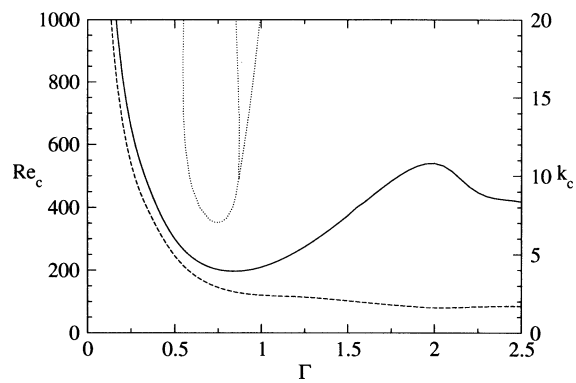

Fig. 3. Critical Reynolds numbers Re_c (solid line) and wave numbers k_c (dashed line) as functions of the aspect ratio Γ. The dotted curve indicates the pure two-dimensional stability boundary ($k = 0$). The rightmost dotted line is the upper bound on Γ for the existence of finite-amplitude two-dimensional flow with broken mirror symmetry [22].

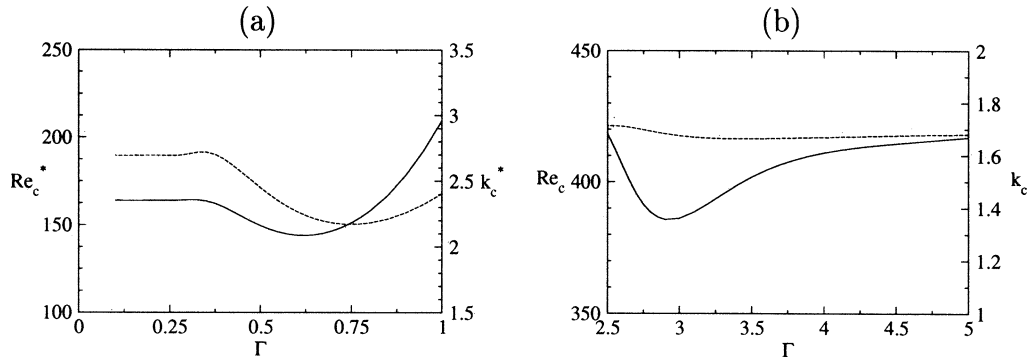

Fig. 4. Rescaled critical Reynolds number $\mathrm{Re}_c^* = \mathrm{Re}_c\,\Gamma$ (solid line) and wave number $k_c^* = k_c\,\Gamma$ (dashed line) as functions of the aspect ratio Γ for small aspect ratios (a), and critical Reynolds numbers Re_c (solid line) and wave number k_c (dashed line) as functions of Γ for large aspect ratios (b).

Table 1
Critical values of the Reynolds number Re_c and wave number k_c for several aspect ratios

Γ	Re_c	k_c
0.2	819.9 ± 8.8	13.48 ± 0.01
0.5	299.2 ± 1.4	4.900 ± 0.005
1.0	209.5 ± 0.6	2.404 ± 0.002
1.5	374.3 ± 1.6	2.048 ± 0.002
2.0	540.1 ± 6.7	1.608 ± 0.005
2.5	418.3 ± 10.7	1.712 ± 0.018

Table 2
Normalized energy production terms for several aspect ratios

Aspect ratio	$\Gamma = 0.30$	$\Gamma = 1.00$	$\Gamma = 1.95$
Reynolds number	$\mathrm{Re}_c = 547.6$	$\mathrm{Re}_c = 209.5$	$\mathrm{Re}_c = 539.0$
i	$\int I_i \,\mathrm{d}V$	$\int I_i \,\mathrm{d}V$	$\int I_i \,\mathrm{d}V$
1	0.264	0.306	0.686
2	−0.154	−0.341	−0.495
3	0.849	0.826	0.871
4	0.043	0.212	−0.048

leftmost dotted stability boundary. Following the stability boundary for increasing Γ a sharp minimum occurs. For still larger values of Γ another dotted line branches from the linear stability boundary at $\Gamma = 0.871$ and $\mathrm{Re} = 497$ [22]. For larger Reynolds numbers the bifurcation to the asymmetric two-dimensional flow is subcritical. The rightmost dotted line indicates the existence boundary of the asymmetric finite-amplitude flow [22]. Note that the three-dimensional linear stability boundary for $\Gamma \lesssim 1$ has a similar shape with a minimum of $\mathrm{Re}_c = 196.3 \pm 0.4$ at $\Gamma = 0.842 \pm 0.001$ as the linear stability boundary for pure two-dimensional perturbations.

3.2. Flow patterns and mechanisms

Albensoeder et al. [17,21] have shown that the instability for large Γ is due to centrifugal effects which are associated with the wall jets emanating from the downstream corners of the moving lids. The wall jets rapidly separate from the rigid wall and high-speed fluid is found on the concave side of the curved streamlines near the separation region. Such local flow conditions are centrifugally unstable. This interpretation is supported by the two sharp peaks of the local energy transfer rate $I = \sum I_i$ which are stretched along the streamlines just in this area. Note that all other contributions to the energy transfer are much smaller. In particular, there is no notable energy transfer in the vortex cores at any cross-section.

When the aspect ratio is decreased from large values, both vortices approach each other and the critical Reynolds number increases. At $\Gamma = 1.983 \pm 0.006$ and $\mathrm{Re}_c = 540.4 \pm 6.6$ it takes a local maximum. The situation is illustrated in Fig. 5 for

$\Gamma = 1.95$. Obviously, the centrifugal instability mechanism is not as efficient for this aspect ratio than for $\Gamma \to \infty$. One reason for the local maximum of $\mathrm{Re}_c(\Gamma)$ could be the incompatibility of the critical flow structures of the individual vortices when they get closer. Nevertheless, the instability mechanism is still of centrifugal type. This interpretation is supported by the criterion proposed by Sipp and Jacquin [23] which gives a sufficient condition for the instability of inviscid two-dimensional rotating flows. According to their criterion which reduces, in the present case, to that of Bayly [24] the inviscid flow in a non-rotating frame of reference is unstable if there exists a streamline for which

$$\frac{|\boldsymbol{u}_0|\omega_0}{R} < 0, \tag{13}$$

for all points $\boldsymbol{x}$ along a closed streamline. Here $|\boldsymbol{u}_0|$ is the absolute value of the velocity, ω_0 the vorticity, and R the local radius of curvature of the streamline of the basic flow ($R > 0$, if the flow is locally counterclockwise, and vice versa). This criterion does not apply to viscous flows. However, a centrifugal instability in viscous flow is promoted if streamlines exist which lie entirely in the region defined by (13). While such streamlines cannot exist in the driven cavity flow, due to the sign of the vorticity near the moving walls, we find that for $\Gamma = 1.95$ there exist streamlines which are almost contained within the region defined by (13). This is shown in Fig. 6(c). Note that the regions of maximum energy transfer to the critical mode (Fig. 5) lie within the gray-shaded area of Fig. 6(c) consistent with the interpretation as a centrifugal instability.

When the aspect ratio is further decreased the critical Reynolds number decreases again. This destabilization of the basic flow is associated with a continuous change of the instability mechanism. As can be seen in Fig. 7(a) for $\Gamma = 1$ the energy transfer to the critical mode is peaked in three distinct regions of the flow. One region of local energy amplification due to $I_1 = -uu\,\partial u_0/\partial x$ (Fig. 7(b)) is symmetrically located in the region of plane straining motion where both jets, originating from the downstream corners of the moving walls, collide. This local amplification is a result of the merging, upon a decrease of Γ, of the two centrifugally unstable regions (Fig. 5). This is confirmed by Fig. 6(b) which shows that the local flow in the

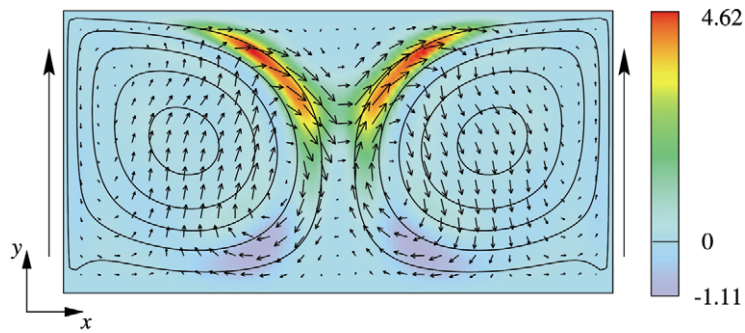

Fig. 5. Streamlines of the basic flow (full lines) for $\Gamma = 1.95$, $\mathrm{Re} = \mathrm{Re}_c = 539.0$, and $k_c = 1.633$, critical mode (arrows), and, in color, the total local production $I = \sum I_i$ in a plane $z = \text{const.}$ in which I takes its maximum value. The side arrows indicate the direction of wall motion.

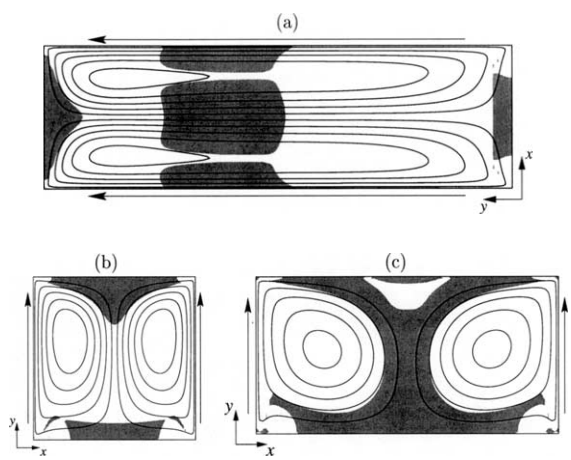

Fig. 6. Regions of the basic flow (gray-shaded) which are prone to centrifugal instability according to the criterion (13). Shown are basic state streamlines at the critical Reynolds number for aspect ratios $\Gamma = 0.30$ (a), $\Gamma = 1.0$ (b), and $\Gamma = 1.95$ (c).

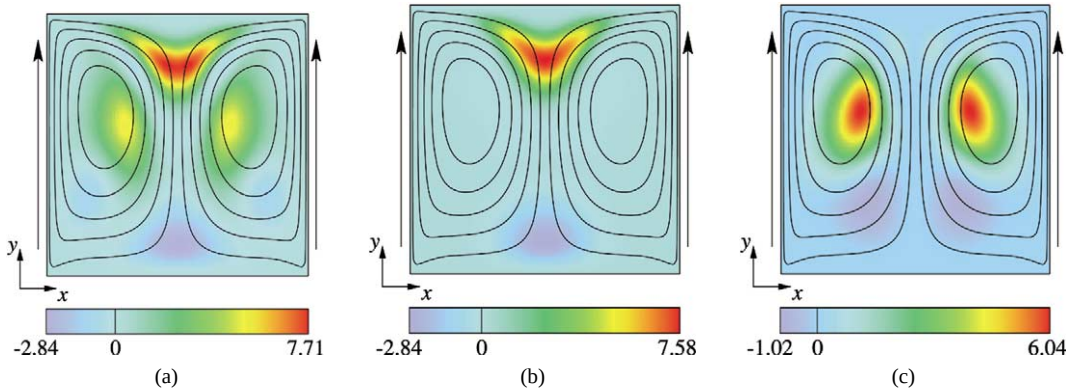

Fig. 7. Streamlines of the basic flow for $\Gamma = 1$, $\mathrm{Re} = \mathrm{Re}_c = 209.5$ with $k_c = 2.404$ and (in color) the total local production (a), local production I_1 (b), and local production I_3 (c) in a plane $z = \text{const.}$ in which the total local production takes its maximum. In this plane $w = 0$.

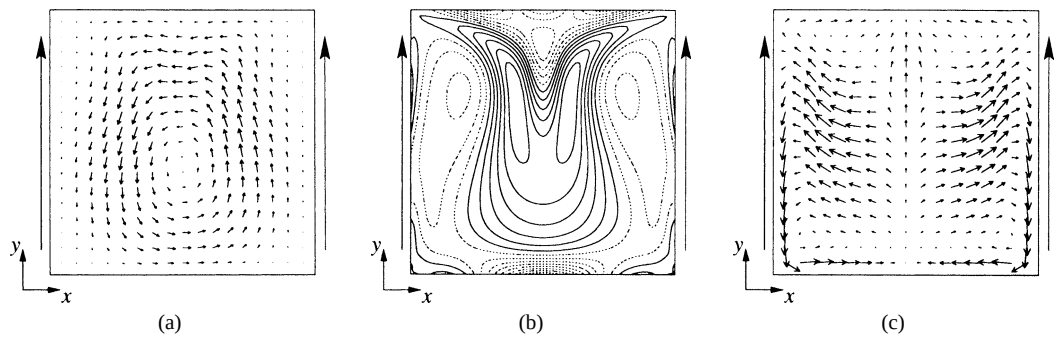

Fig. 8. (a) Critical velocity field $\boldsymbol{u}$, (b) isolines of the disturbance vorticity ω_z in z-direction, and (c) projection of the critical vorticity field $\boldsymbol{\omega}$ for $\Gamma = 1$ and $\mathrm{Re} = \mathrm{Re}_c = 209.5$ with $k_c = 2.404$. The parameters and projection planes are the same as in Fig. 7, except for the projection plane in (c) which is shifted by a quarter wave length.

region of maximum energy transfer is prone to centrifugal effects, since (13) is locally satisfied. The major contribution to the local energy transfer is due to the deceleration of the jets ($\sim \partial u_0/\partial x$) approaching the stagnation point $(x, y) = (0, 1/2)$. The opposing process is found near the bottom stagnation point $(x, y) = (0, -1/2)$ where the acceleration of the flow in x direction yields a stabilization.

Two more regions of local energy transfer are visible in Fig. 7(c) near the vortex cores. Centrifugal effects are not operating in this region of the flow, since the local flow does not satisfy criterion (13). The energy-transfer peaks are rather caused by the straining of both vortex cores when the aspect ratio becomes less than two, giving rise to a significant energy transfer $I_3 = -vu\,\partial v_0/\partial x$. The local energy transfer I_3 by transport of streamwise momentum perpendicular to the direction of the basic flow is very similar as in the elliptical instability of a single strained vortex [18,21]. As a characteristic feature it can be seen from Fig. 8(a) that the perturbation velocity vectors make angles of approximately 45° with the streamlines. Both of the destabilizing actions, centrifugal effects and strain, work together such that the critical mode at a fixed spanwise location $z = \text{const.}$ takes the form of a single vortex centered in the cavity (Fig. 8(a)). Since the sense of rotation of the perturbation vortex flow changes with a period $2\pi/k_c$ both basic vortices are equally effected and alternatingly displaced such that one vortex core is shifted towards the hyperbolic stagnation point $(x, y) = (0, 1/2)$ of the converging flow region, while the other vortex is shifted away from this point.

The vorticity of the critical mode is shown in Figs. 8(b) and 8(c). In the plane in which $w = 0$ and where the energy transfer takes its maximum, the z-component of the vorticity approximately exhibits a dipolar structure in each vortex core (Fig. 8(b)), which is characteristic for the elliptic instability [25]. In the plane in which $\partial w/\partial z = 0$, shown in Fig. 8(c), we find that the vorticity is nearly aligned with the strain associated with the elliptical deformation in y-direction of both vortex cores. Accordingly, $\boldsymbol{\omega}$ makes an angle of approximately 45° with respect to the y-axis, parallel to the principal axes of the strain.

Apart from the periodicity in z-direction, the displacement of the basic vortices is very similar as for the pure two-dimensional mirror-symmetry-breaking instability for $\Gamma \approx 0.75$ (dotted lines in Fig. 3). In fact, we find that the velocity component w of the three-dimensional critical mode for $\Gamma = 1$ is much smaller than u and v. Hence, the perturbation flow is nearly two-dimensional. The similarity of the three- and two-dimensional neutral modes becomes clear if one realizes that

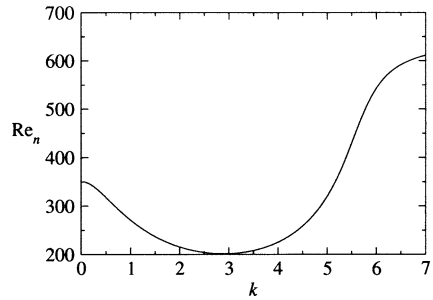

Fig. 9. Neutral Reynolds number Re_n as function of the wave number k for $\Gamma = 0.75$.

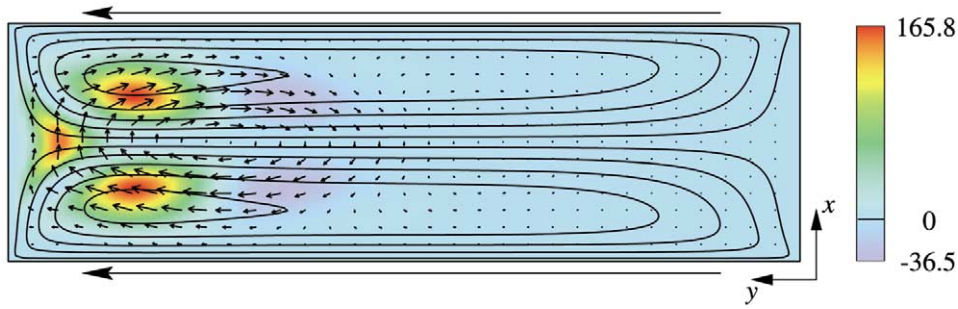

Fig. 10. Streamlines of the basic flow for $\Gamma = 0.30$, $\mathrm{Re} = \mathrm{Re}_c = 547.6 \pm 3.7$ (full lines), critical mode (arrows), and total local energy production (color) in the plane $z = \text{const.}$ where $w = 0$ and in which the total local production takes its maximum. The critical wave number is $k_c = 9.018 \pm 0.005$.

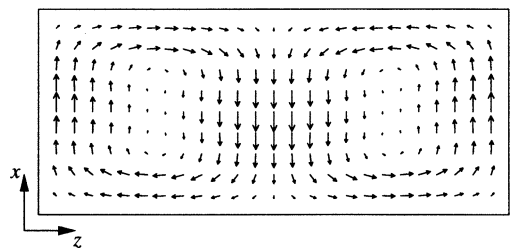

Fig. 11. Critical velocity field for $\Gamma = 0.30$ at $\mathrm{Re} = \mathrm{Re}_c = 547.6$ shown over one period $2\pi/k_c$ in the plane $y = 0.34$ where the total local production takes its maximum.

both modes are connected with each other, at least for a certain range of Γ, through a neutral curve $\mathrm{Re}_n(k)$. An example for $\Gamma = 0.75$ is shown in Fig. 9.

The character of the critical mode does not change when the aspect ratio is further decreased. The production terms $\int I_1 \,\mathrm{d}V$ and $\int I_3 \,\mathrm{d}V$ remain the most important positive contributions to the energy budget. However, the relative magnitude of the z component of the perturbation velocity becomes much larger than for $\Gamma = 1$. A typical critical mode is shown in Fig. 10 for $\Gamma = 0.30$. In the cavity half upstream of the moving walls ($y < 0$) the perturbation flow is very weak. The critical mode is concentrated at the downstream end of the cavity. In this region the streamlines converge near the stagnation point $(x, y) = (0, 1/2)$ and the fluid is stretched along the outgoing streamline $x = 0$. Therefore, one might also consider the possibility of a hyperbolic instability, as for plane hyperbolic stagnation-point flow [26]. The most dangerous perturbation in hyperbolic stagnation-point flow is amplified by vortex stretching into the direction of the outgoing streamline. In the present cavity flow we find that the y component of the perturbation vorticity is significant near the stagnation point of the converging flow (Fig. 11), but it disappears rapidly further downstream from the stagnation point. The vorticity significantly diminishes for $y = 0$, where the flow has already become nearly parallel. We conclude that vortex stretching in z-direction can operate only over a short distance in y and is of minor importance here.

From Fig. 4(a) the critical Reynolds number $\mathrm{Re}_c^* = 164.3 \pm 1.1$ for $\Gamma = 0.30$ appears to be very close to the asymptotic value which is estimated as $\mathrm{Re}_c^*(\Gamma \to 0) = 164 \pm 6$. It can be expected, therefore, that the structure of the critical mode for $\Gamma = 0.3$ is a very good approximation to the critical mode for $\Gamma \to 0$.

4. Discussion and conclusion

The linear stability of the two-dimensional incompressible flow of two symmetric counter-rotating vortices in a two-sided lid-driven cavity has been calculated. The centrifugal instability when both vortices are distant ($\Gamma \gg 1$) merges smoothly, for decreasing Γ, to an instability in which flow deceleration and straining of the vortex cores are the determining factors. In shallow cavities ($\Gamma \ll 1$) the critical modes are strongly localized near the downstream end of the cavity.

While the centrifugal instability for $\Gamma \gtrsim 2$ is clearly due to the deceleration of the flow along the outer streamlines owing to the presence of the rigid walls [17], the combined instability for $\Gamma \lesssim 1$ is significantly effected by the strain in the vortex cores. It is then natural to compare the present instabilities with those of strained vortices in unbounded flows. The prototype of such a flow is a strained Rankine vortex [27–29]. The generic instability of a Rankine vortex in a weak dipolar strain field occurs at those axial wave numbers at which the rotation rates of the natural oscillations (Kelvin waves) vanish. The first resonances (instabilities) occur at $k = 0$ (long-wave instability) and at $k = 2.5/a$ (short-wave instability), where a is the radius of the Rankine vortex (see, e.g., [30]). Both instabilities have recently been observed by [31] to occur simultaneously on a pair of counter-rotating vortices which mutually impose a strain field on each other.

The long-wave mode, which is symmetric with respect to $x = 0$, is also known as the Crow instability [32]. This instability dominates in the limit of slender vortices when $b/a \gg 1$, where b is the separation of both vortices. In the present setup this limit would correspond to $\Gamma \gg 1$. However, we did not find long-wave modes for any value of Γ. The reason probably is that for $\Gamma \gg 1$ one vortex in the cavity cannot effectively induce a strain on the other vortex, because a long-range flow field is absent and the interaction between both vortices is exponentially weak. They are only coupled through the viscous Moffatt eddies [3] between the parallel rigid walls. We conclude that the presence of the rigid walls prevents the long-wave instability in large aspect-ratio cavities.

The short-wave cooperative mode is antisymmetric with respect to $x = 0$. We find that the critical mode in the cavity for $\Gamma \lesssim 1$ exhibits the same symmetries as the cooperative instability on an unbounded vortex pair. Moreover, the main qualitative flow structures of the perturbations, i.e. the dipolar structure of the vorticity in the vortex core and the orientation of the perturbation vorticity, are very similar (compare, e.g., Figs. 7 and 8 with Figs. 5 and 10 of [31]). If we estimate the typical vortex-core radius for $\Gamma \lesssim 1$ as $a \approx \Gamma/4$ the wave number of the cooperative short-wave instability of a corresponding Rankine vortex would be $k \approx 10/\Gamma$. However, the actual critical wave number in the cavity is much smaller (see Fig. 4(a)). Hence, we conclude that the instability of the cavity flow with parallel wall motion shows the same qualitative features as the cooperative short-wave instability of strained vortices in unbounded flows. Both systems differ in that the strain in the vortex cores of the cavity flow is not simply induced by well-defined vortex patches (like the Rankine vortices) but strongly influenced by the geometrical constraints and the tangential velocity distribution on the walls. Finally, the flow-deceleration effect near the separation point at $(x, y) = (0, 1/2)$ may also alter the cooperative instability to some degree.

The instabilities studied here can also arise in other variants of the lid-driven cavity problem. Nienhüser et al. [33], for example, considered the stability of steady axisymmetric toroidal vortices in low-Prandtl-number thermocapillary liquid bridges. For $\Gamma = 1$ they found a stationary instability which is likewise driven by a centrifugal and a straining mechanism. The spatial distributions of the respective energy-transfer rates are very similar to those in the lid-driven cavity flow.

The transition to time-dependence and to turbulent flow is still an open problem, and it must be investigated by full three-dimensional simulations. It would be interesting to compare the corresponding scenarios with the recent observations of the transient decay of a vortex pair made by [31].

Acknowledgement

This work has been supported by DFG through grant number Ku896/8-1 and Ku896/5-2.

References

[1] M. Deville, T.-H. Lê, Y. Morchoisne, in: Numerical Simulation of 3-D Incompressible Unsteady Viscous Laminar Flows, Notes on Numerical Fluid Mechanics, Vol. 36, Vieweg, Braunschweig, 1992.

[2] O.R. Burggraf, Analytical and numerical studies of the structure of steady separated flows, J. Fluid Mech. 24 (1966) 113–151.

[3] H.K. Moffatt, Viscous and resistive eddies near a sharp corner, J. Fluid Mech. 18 (1964) 1–18.
[4] F. Pan, A. Acrivos, Steady flows in rectangular cavities, J. Fluid Mech. 28 (1967) 643–655.
[5] M.A. Kelmanson, B. Lonsdale, Eddy genesis in the double-lid-driven cavity, Quart. J. Mech. Appl. Math. 49 (1996) 635–655.
[6] J.R. Koseff, R.L. Street, The lid-driven cavity flow: A synthesis of qualitative and quantitative observations, J. Fluids Eng. 106 (1984) 390–398.
[7] E. Leriche, S. Gavrilakis, Direct numerical simulation of the flow in a lid-driven cubical cavity, Phys. Fluids 12 (2000) 1363–1376.
[8] J.R. Koseff, R.L. Street, Visualization studies of a shear driven three-dimensional recirculating flow, J. Fluids Eng. 106 (1984) 21–29.
[9] J.R. Koseff, R.L. Street, On endwall effects in a lid-driven cavity flow, J. Fluids Eng. 106 (1984) 385–389.
[10] A.K. Prasad, J.R. Koseff, Reynolds number and end-wall effects on a lid-driven cavity flow, Phys. Fluids A 1 (1989) 208–218.
[11] C.W. Leong, J.M. Ottino, Experiments on mixing due to chaotic advection in a cavity, J. Fluid Mech. 209 (1989) 463–499.
[12] P.N. Shankar, M.D. Deshpande, Fluid mechanics in the driven cavity, Annu. Rev. Fluid Mech. 32 (2000) 93–136.
[13] M. Poliashenko, C.K. Aidun, A direct method for computation of simple bifurcations, J. Comput. Phys. 121 (1995) 246–260.
[14] N. Ramanan, G.M. Homsy, Linear stability of lid-driven cavity flow, Phys. Fluids 8 (1994) 2690–2701.
[15] Y. Ding, M. Kawahara, Linear stability of incompressible fluid flow in a cavity using finite element method, Internat. J. Numer. Methods Fluids 27 (1998) 139–157.
[16] Y. Ding, M. Kawahara, Three-dimensional linear stability analysis of incompressible viscous flows using the finite element method, Internat. J. Numer. Methods Fluids 31 (1999) 451–479.
[17] S. Albensoeder, H.C. Kuhlmann, H.J. Rath, Three-dimensional centrifugal-flow instabilities in the lid-driven cavity problem, Phys. Fluids 13 (2001) 121–135.
[18] H.C. Kuhlmann, M. Wanschura, H.J. Rath, Flow in two-sided lid-driven cavities: Non-uniqueness, instabilities, and cellular structures, J. Fluid Mech. 336 (1997) 267–299.
[19] H.C. Kuhlmann, M. Wanschura, H.J. Rath, Elliptic instability in two-sided lid-driven cavity flow, Eur. J. Mech., B/Fluids 17 (1998) 561–569.
[20] C. Blohm, H.C. Kuhlmann, The two-sided lid-driven cavity: Experiments on stationary and time-dependent flows, J. Fluid Mech. 450 (2002) 67–95.
[21] S. Albensoeder, H.C. Kuhlmann, Linear stability of rectangular cavity flows driven by anti-parallel motion of two facing walls, J. Fluid Mech. 458 (2002) 153–180.
[22] S. Albensoeder, H.C. Kuhlmann, H.J. Rath, Multiplicity of steady two-dimensional flows in two-sided lid-driven cavities, Theor. Comput. Fluid Dyn. 14 (2001) 223–241.
[23] D. Sipp, L. Jacquin, Three-dimensional centrifugal-type instabilities of two-dimensional flows in rotating systems, Phys. Fluids 12 (2000) 1740–1748.
[24] B.J. Bayly, Three-dimensional instability of elliptical flow, Phys. Rev. Lett. 57 (1986) 2160–2163.
[25] F. Waleffe, On the three-dimensional instability of strained vortices, Phys. Fluids A 2 (1990) 76–80.
[26] R.R. Lagnado, N. Phan-Thien, L.G. Leal, The stability of two-dimensional linear flows, Phys. Fluids 27 (1984) 1094–1101.
[27] C.-Y. Tsai, S.E. Widnall, The stability of short waves on a straight vortex filament in a weak externally imposed strain field, J. Fluid Mech. 73 (1976) 721–733.
[28] M.J. Landman, P.G. Saffman, The three-dimensional instability of strained vortices in a viscous fluid, Phys. Fluids 30 (1987) 2339–2342.
[29] S.L. Dizés, C. Eloy, Short-wavelength instability of a vortex in a multipolar strain field, Phys. Fluids 11 (1999) 500–502.
[30] P.G. Saffman, Vortex Dynamics, Cambridge University Press, 1992.
[31] T. Leweke, C.H.K. Williamson, Cooperative elliptic instability of a vortex pair, J. Fluid Mech. 360 (1998) 85–119.
[32] S.C. Crow, Stability theory for a pair of trailing vortices, AIAA J. 12 (1970) 2172–2179.
[33] C. Nienhüser, H.C. Kuhlmann, Stability of thermocapillary flows in non-cylindrical liquid bridges, J. Fluid Mech. 458 (2002) 35–73.